Insight into the Catalytic Reduction of NO by Methane: The Reaction of Nitromethane on Oxidized Mo(110)

Ally S. Y. Chan, L. Jay Deiner, and C. M. Friend*

Harvard University, Department of Chemistry, 12 Oxford Street, Cambridge, Massachusetts 02138

Received: June 14, 2002; In Final Form: September 11, 2002

The reactions of nitromethane (CH_3NO_2) on a thin-film oxide grown on Mo(110) are investigated to gain insight into the role of nitromethane in the catalytic reduction of NO by methane. Using a combination of temperature programmed reaction and infrared reflection-absorption spectroscopy, we find that nitromethane reacts by dissociation of the N-O bonds below 300 K, to yield methylimido (CH_3N_{ads}) and terminally-bound oxygen (Mo═O). Methylimido is stable on the surface up to ∼550 K. Dehydrogenation of CH_3N to form HCN and H_2O is the major pathway; homolytic C−N bond fission to yield gaseous methyl radicals and formaldehyde are minor pathways. Formaldehyde is proposed to form from addition of some methyl radicals to surface oxygen, forming transient methoxy (CH_3O), which dehydrogenates to form formaldehdye. Overall, C−N bond retention is favored in the reaction of nitromethane on the thin-film oxide on Mo(110). These results are discussed in the general framework of the CH_4-assisted reduction of NO.

Introduction

The chemistry of nitromethane on metal and oxide surfaces is of interest due to its importance in environmental[1] and industrial[2,3] catalytic processes. Of particular significance is the possible role of nitromethane as an intermediate in the selective catalytic reduction of nitrogen oxides, NO_x, by methane[4−7] and other hydrocarbons.[8] Current technology for limiting NO_x emissions relies mainly on the use of NH_3 as a reductant, which presents serious cost and hazard issues.[1] Moreover, NH_3 is not a feasible reducing agent for NO_x emissions from automobile exhausts. The selective catalytic reduction of NO_x by methane is, therefore, a promising alternative to controlling NO_x emissions, as it employs residual hydrocarbons already present in exhaust emissions.

Despite substantial evidence that methane enhances NO_x reduction over a variety of catalysts, including zeolites,[9,10] rare earth oxides,[11,12] and metal-promoted oxides,[12,13] the mechanism for this process is still not well understood. One possibility is that methyl radicals formed from methane would scavenge surface oxygen deposited from NO dissociation, which would otherwise deactivate the catalyst by occupying sites required for NO reduction. Alternatively, under lean-burning (oxygen-rich) conditions, NO may be oxidized to a more effective oxidant, NO_2, that is capable of activating the C−H bond in methane, thus generating $\bullet CH_3$:[7,14]

$$2NO + O_2 \rightarrow 2NO_2$$

$$CH_4 + NO_2 \rightarrow \bullet CH_3 + HONO \text{ (or } OH + NO)$$

Methyl radicals are proposed to react directly with NO_2 to form a nitromethane intermediate:[4−7]

$$\bullet CH_3 + NO_2 \rightarrow CH_3NO_2$$

Once nitromethane is formed, there are a number of possible routes for reaction, some of which will yield oxygenates and N_2 or N_2O. For example, nitromethane decomposes to ammonia and CO_2 on metal-doped zeolites, e.g., Co-ZMS5[14,15] and Cu−ZSM5.[4] Ammonia would then react in one or more of the following ways to yield N_2 and/or N_2O:

$$2NH_3 + 2NO_2 \rightarrow N_2 + N_2O + 3H_2O$$

$$4NH_3 + 3O_2 \rightarrow 2N_2 + 6H_2O$$

$$4NH_3 + 4NO + O_2 \rightarrow 4N_2 + 6H_2O$$

Direct reaction of nitromethane with NO_2 may also occur,[14] leading to the desired NO reduction products:

$$8CH_3NO_2 + 6NO_2 \rightarrow 7N_2 + 8CO_2 + 12H_2O$$

At the same time, HCN and water formation were reported for nitromethane reaction over these zeolites, indicating that undesirable side reactions compete with NO_x reduction.

Fundamental studies of nitromethane reactions under well-defined conditions can provide insight into the elementary steps leading to formation of the various products of nitromethane decomposition, and the specific characteristics of the catalyst surface that may favor the desired products. To this end, both homogeneous nitromethane reactions and heterogeneous reactions on metal surfaces have been the subject of considerable study. Nitromethane undergoes reversible molecular adsorption on Au(111)[16,17] and Pt−Sn surface alloys,[18] while reaction by N−O bond dissociation and C−N bond retention to yield HCN is favored on Pt(111)[19] and Ni surfaces.[20,21] On Rh(111)[22] and polycrystalline Pt foils,[23] cleavage of both C−N and N−O bonds occur upon adsorption at 300 K, leading to complete decomposition of the molecule. In contrast, homogeneous nitromethane reactions proceed via markedly different pathways. Homolytic C−N bond fission to yield $\bullet CH_3$ and NO_2 is proposed to be the rate-determining step in the thermal decomposition of nitromethane in the gas phase[24,25] and in solution.[26] However, potential energy surface calculations by Dewar et al.[27] predicted that nitromethane would decompose most easily by initial rearrangement to methyl nitrite (CH_3ONO), as the activation

10.1021/jp021429a CCC: $22.00
Published on Web 12/03/2002

energy for rearrangement is significantly less than that for C−N homolysis. Indeed, products attributable to both isomerization and C−N bond fission pathways, with an isomerization: homolysis branching ratio of 1:0.6 were reported in a later study of nitromethane decomposition in a collision-free environment.[28]

In this study, we have investigated the reactions of nitromethane on a thin-film oxide formed on Mo(110). The thin-film oxide on Mo(110) is chosen as a model substrate, since the addition of Mo to alumina-supported catalysts has been shown to enhance their activity toward NO reduction by hydrocarbons.[29] Moreover, N−N bond formation via NO coupling to dinitrosyls on MoO_3 has been implicated in the improved activity for NO reduction on MoO_3-promoted Pt-group catalysts.[30,31] On the thin-film oxide, we find that nitromethane decomposes by scission of the N−O bonds to deposit oxygen primarily in terminal (atop) sites. Decomposition of the resulting CH_3N intermediate yields HCN and H_2O as major products, with some $\bullet CH_3$ and CH_2O also produced by dissociation of C−N bonds. Nitrogen from C−N bond scission remains chemisorbed to the thin-film oxide and subsequently recombines to evolve N_2 at ∼1250 K. Notably, the fact that C−N bond retention is favored and formaldehyde production is a minor pathway suggest that the conversion of CH_3NO_2 to oxygenates of carbon is not efficient on the thin-film oxide on Mo(110). Moreover, the high temperature for N_2 evolution indicates that the thin-film oxide is not a viable catalyst for NO reduction via a nitromethane intermediate due to its propensity for strong chemisorption of nitrogen. Taken together with previous studies on the surface reactions of nitromethane, these results illustrate that oxophilic substrates may in part be responsible for the absence of NO reduction products from nitromethane, by promoting the dissociation of N−O bonds over C−N bonds.

Experimental Section

All experiments were performed in two ultrahigh vacuum chambers with base pressures below 1×10^{-10} Torr, which have been described elsewhere.[32,33] Briefly, each chamber is equipped with low energy electron diffraction (LEED) optics, a cylindrical mirror analyzer with concentric electron gun for Auger electron spectroscopy, and a quadrupole mass spectrometer (1−300 amu) capable of sampling up to 16 masses in a single temperature programmed reaction experiment.[34] The first chamber houses an electron energy loss spectrometer while the second is interfaced with a Fourier transform infrared spectrometer for infrared reflection−absorption spectroscopy.

The Mo(110) crystal was cleaned by oxidation at 1200 K in 1×10^{-9} Torr of O_2 for 5 min, followed by repeated flashing to 2300 K to remove the residual oxide. No surface carbon or oxygen was detected by Auger electron spectroscopy and a sharp (1×1) LEED pattern was obtained following this procedure. The thin-film oxide with no terminal oxygen present was used in this investigation. In this thin-film oxide, oxygen occupies low symmetry, high coordination sites on the surface and in the lattice;[35,36] however, some oxygen vacancies at high coordination sites on the surface are also created during the preparation procedure. Preparation of the thin-film oxide is achieved by exposure to 1×10^{-9} Torr of O_2 for 5 min with the crystal temperature held at 1200 K, followed by annealing to 1400 K for 10 s in a vacuum. The high temperature used for oxidation induces transport of oxygen into the lattice. Flashing to 1400 K in a vacuum after oxidation completely depopulates terminally bound oxygen, and also creates oxygen vacancies at high coordination sites. Characterization of the thin-film oxide has been described in detail elsewhere.[37,38]

Oxygen (O_2, 99.998%, Matheson) and isotopically labeled oxygen ($^{18}O_2$, 95−98%, Cambridge Isotope Labs) were used without further purification. Several isotopomers of nitromethane—CH_3NO_2, $^{13}CH_3NO_2$, and CD_3NO_2, (all 99% purity, Sigma-Aldrich)—were subjected to several freeze−pump−thaw cycles prior to use and their purities verified by mass spectrometry.

Nitromethane was dosed using a directed doser positioned ∼5 mm away from the crystal surface. The crystal was biased at −70 V during dosing to eliminate electron-induced reactions of nitromethane on the surface, due to stray electrons originating from the ion gauge. Without the bias, the current from the ion gauge to the crystal was ∼0.1 nA. In addition, temperature programmed reaction data of nitromethane dosed *without* applying a −70 V bias showed the evolution of N-containing products below 200 K: predominantly N_2O and N_2, and a small amount of NO. These products are attributed to an electron-induced reaction of adsorbed nitromethane, based on their absence in the temperature programmed reaction data when a −70 V bias was applied during dosing. Radiative heating to 800 K ($dT/dt \sim 10$ K s^{-1}) was used in all temperature programmed reaction experiments. Electron bombardment heating, with approximately the same heating rate, was used to collect temperature programmed reaction data above 800 K.

Results

Temperature-Programmed Reaction. Competition between desorption and reaction is observed during temperature programmed reaction of nitromethane on the thin-film oxide formed on Mo(110). Molecular desorption of CH_3NO_2 ($m/z = 61$) peaks at 180 K and accounts for ∼20% of nitromethane from the first monolayer (Figure 1a, inset). At high coverages, CH_3NO_2 multilayers condensed on the surface sublime in a peak at 150 K. This peak grows indefinitely with increasing CH_3NO_2 exposure, and is at a similar temperature to that reported on other surfaces.[17−19] Saturation coverage is defined as the exposure of nitromethane just below the onset of CH_3NO_2 multilayer sublimation, where all product peaks have achieved their maximum intensity at this exposure.

The primary reaction products detected during temperature programmed reaction of nitromethane are HCN and H_2O, evolved concomitantly in peaks at 695 K (Figure 1a). In addition, lesser amounts of methyl radicals ($\bullet CH_3$), methane (CH_4), and formaldehyde (CH_2O) are evolved in peaks at ∼675 K. No other products are detected in an extensive mass search between 2 and 100 amu in temperature programmed reaction up to 800 K. In particular no N−N coupling products, i.e., N_2 and N_2O, are detected based on the absence of peaks at $m/z = 28$ and 44, respectively. All products are identified by quantitative comparison of integrated peak intensities with the intensities of mass spectral cracking fragments measured for authentic samples, in conjunction with isotopic shifts in masses observed during isotopic labeling experiments (Table 1).

Water and HCN are evolved in comparable yields at the same peak temperature of 695 K, and with similar peak shapes (Table 1, Figure 1). The similarities in yield, peak temperature and shape for these two products suggest that they are derived from a common intermediate, with the same rate-determining step leading to their production. The rate-determining step is identified to be C−H bond scission, based on the ∼10 K increase in peak temperature for both D_2O and DCN production from CD_3NO_2 reaction on the thin-film oxide, relative to HCN and H_2O formation from CH_3NO_2 (Figure 1b).

Isotopic labeling of the thin-film oxide demonstrates that water is formed from reaction with surface-bound oxygen, and

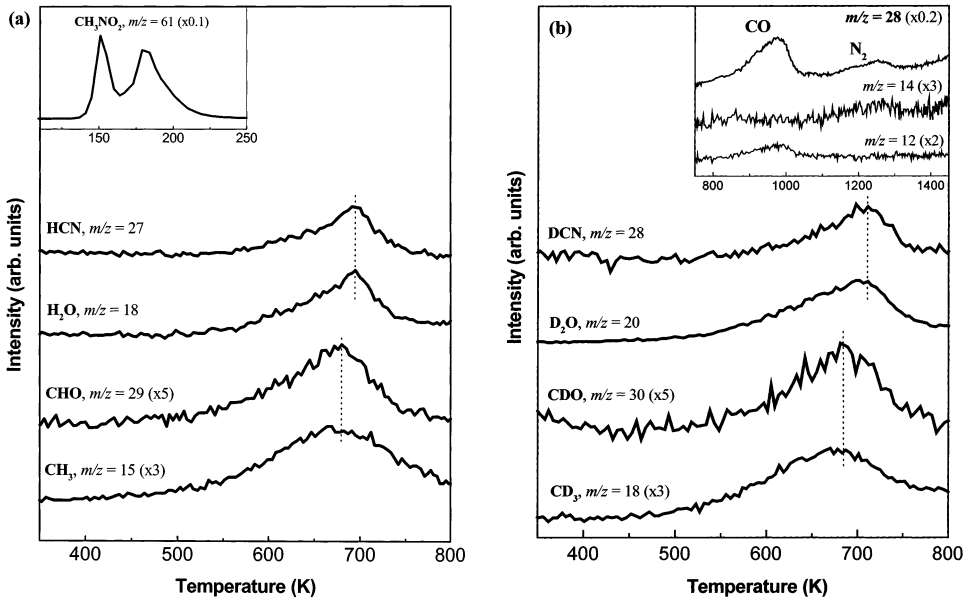

Figure 1. Temperature programmed reaction data obtained after adsorption of a saturation coverage of (a) CH_3NO_2, and (b) CD_3NO_2 on the thin-film oxide formed on Mo(110). The inset in (a) shows molecular CH_3NO_2 desorption at 180 K (monolayer) and 150 K (multilayer); for a high CH_3NO_2 coverage on the thin-film oxide. The inset in (b) shows recombinant CO and N_2 production from nonselective decomposition of CD_3NO. The $m/z = 18$ trace in (b) is corrected for contribution from OD^+ from D_2O formation.

TABLE 1: Comparison of Mass Fragmentation Patterns of Authentic Samples with Temperature Programmed Reaction Products from CH_3NO_2 and CD_2NO_2 Reactions on the Thin-Film Oxide

	intensity at *m/z*												
	15	16	17	18	19	20	26	27	28	29	30	31	32
molecule													
hydrogen cyanide[a]							28	100					
water[a]		2	30	100									
methane[a]	81	100											
formaldehyde[b]	3								24	100	62		
ethane[b]	7						25	36	100	21	23		
methyl radical[a] (from methanol decomposition on the thin-film oxide)	100	74											
products													
(1) CH_3NO_2/^{16}O-thin-film oxide	33	25	34	112			30	100	5	20	13		
residual after subtraction of HCN and H_2O signals, leaving $\bullet CH_3$ and CH_2O[c] (scaled to $m/z = 29$, $CH^{16}O$)	165	125							25	100	65		
(2) CH_3NO_2/^{18}O-thin-film oxide[d]	34	23	10	31	23	84	29	100		3	6	16	11
residual after subtraction of HCN and H_2O signals, leaving $\bullet CH_3$ and CH_2O[c] (scaled to $m/z = 31$, $CH^{18}O$)	212	143								19	37	100	69
(3) CD_3NO_2/^{16}O-thin-film oxide				61	21	110	32		100		15		9
residual after subtraction of DCN, D_2O and CD_2O signals (scaled to $m/z = 19$, CD_3H)				133	100								

[a] Measured in laboratory spectrometer. [b] Taken from literature (NIST Chemistry Webbook). [c] The residuals at $m/z = 17$ and 26 are within the noise of the instrument. [d] No $CH_3N^{18}O_2$ ($m/z = 65$) and $CH_3N^{16}O^{18}O$ ($m/z = 63$) were detected during desorption of CH_3NO_2 from the ^{18}O-thin-film oxide.

that substantial N−O bond dissociation in nitromethane occurs below 600 K. Both $H_2{}^{16}O$ and $H_2{}^{18}O$ are detected during nitromethane reaction on the ^{18}O-labeled thin-film oxide (Table 1). The ratio of ^{16}O:^{18}O-water is strongly dependent on nitromethane coverage, such that the ratio at low CH_3NO_2 coverage (~30% saturation) is 0.88:1.0, while at saturation coverage the ratio increases approximately 3-fold to 2.7:1. The increase in $H_2{}^{16}O$ yield at saturation coverage is attributed to the larger amount of ^{16}O deposited on the thin-film oxide upon dissociation of the N−O bonds in nitromethane.

Methyl radical evolution ($m/z = 15$) is observed in a peak centered at 675 K (Figure 1a). Although methane ($m/z = 16$) is also detected coincidentally with $\bullet CH_3$, we attribute it entirely to the reaction of $\bullet CH_3$ with background hydrogen in the chamber. The identification of $\bullet CH_3$ is based on the above unity integrated peak intensity ratio, $I(m/z{=}15)$:$I(m/z{=}16)$, which is similar to the ratio measured for $\bullet CH_3$ from CH_3OH reaction on the thin-film oxide for which the generation of methyl radicals has been independently verified (Table 1).[39] In contrast, the $I(m/z{=}15)$:$I(m/z{=}16)$ for methane is measured to be 0.8:1.0 (Table 1). Previous studies of methanol reaction on oxidized Mo(110)[38,39] have shown that gaseous $\bullet CH_3$ is produced, and that it reacts with background hydrogen to form methane. Furthermore, $\bullet CD_3$ ($m/z = 18$) and CD_3H ($m/z = 19$), but no CD_4 ($m/z = 20$), is produced in the temperature programmed reaction of CD_3NO_2 (Table 1), clearly indicating $\bullet CD_3$ reaction

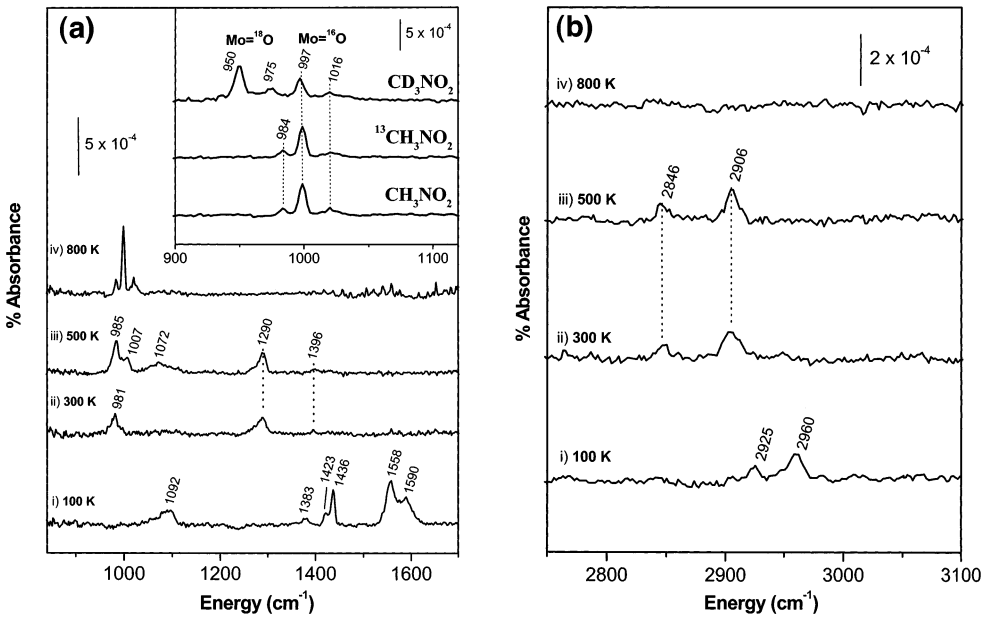

Figure 2. Infrared reflection absorption spectra for a saturation coverage of CH_3NO_2 on the thin film oxide on Mo(110) for various temperatures: (i) as deposited at 100 K and after heating to (ii) 300 K, (iii) 500 K, and (iv) 800 K. Two different spectral regions are shown at (a) 840−1700 cm^{-1}, and (b) 2750−3100 cm^{-1}. The inset in (a) shows the terminal oxygen (Mo═O) region at 800 K for CH_3NO_2 and $^{13}CH_3NO_2$ on the ^{16}O-thin-film oxide, and for CD_3NO_2 on the ^{18}O-thin-film oxide.

with background hydrogen. (The peak at $m/z = 20$ in CD_3NO_2 reaction is found to be entirely due to $D_2{}^{16}O$, with no contribution from CD_4, based on quantitative comparison of this peak to that for $D_2{}^{18}O$ production at $m/z = 22$, from CD_3NO_2 reaction on ^{18}O-labeled thin-film oxide.) Importantly, no kinetic isotopic effect is evident in the production of $\bullet CH_3$ and $\bullet CD_3$ from CH_3NO_2 and CD_3NO_2, respectively; the yield and peak temperature for both products are virtually identical.

A small amount of formaldehyde, CH_2O, is produced at a similar temperature as $\bullet CH_3$ (Figure 1a). The absence of any significant intensity at $m/z = 28$ and $m/z = 48$ rules out any contribution from ethane or formamide ($CHONH_2$), respectively, both of which have overlapping cracking fragments with formaldehyde. The rate-determining step in formaldehyde production is determined to be C−H bond scission, based on the ∼10 K upshift in peak temperature for CD_2O production from CD_3NO_2, compared to CH_2O from CH_3NO_2. Incorporation of surface oxygen into formaldehyde is evident from ^{18}O-labeling of the thin-film oxide. At saturation coverage of nitromethane, the majority of formaldehyde is evolved as $CH_2{}^{18}O$ and $CD_2{}^{18}O$ in the reactions of CH_3NO_2 and CD_3NO_2, respectively, on the ^{18}O-labeled surface, with a small amount of ^{16}O-formaldehyde produced in both cases (Table 1). The low intensities of formaldehyde preclude quantitative comparison of the yields of $CH_2{}^{18}O$ to $CH_2{}^{16}O$. However, the isotopic distribution of oxygen incorporated into formaldehyde, compared to that for water, suggests that the oxygen in formaldehyde must originate from high-coordination sites on the surface that are mainly occupied by ^{18}O on the labeled thin-film oxide, rather than from nitromethane. The minor amount of $CH_2{}^{16}O$ produced is attributed to occupation of ^{16}O from CH_3NO_2 at oxygen vacancies in high-coordination sites that are created during preparation of the thin-film oxide.

Finally, ∼50% of the saturated nitromethane monolayer undergoes nonselective decomposition on the thin-film oxide on Mo(110), based on the evolution of carbon monoxide at 970 K and dinitrogen at 1250 K (Figure 1b, inset). CO and N_2 production, both at $m/z = 28$, can be distinguished by monitoring C^+, at $m/z = 12$, and N^+, at $m/z = 14$, respectively. The proportion of the saturated nitromethane monolayer that completely decomposes is quantified by comparing the CO yield at 970 K to the total yield of products, after accounting for the fraction of nitromethane removed from the surface via molecular desorption (∼20%). Using this analysis, we find that only 30% of the nitromethane monolayer adsorbed on the thin-film oxide at 100 K undergoes selective reaction to yield gaseous products.

TABLE 2: Assignments for Vibrational Bands of Molecular CH_3NO_2

normal mode	CH_3NO_2 on thin film oxide formed on Mo(110)		CH_3NO_2 (solid)[a]	CH_3NO_2 monolayer on Au (111)[b]
	monolayer	multilayer		
$\nu_a(CH)$	2960	3018	3072, 3037	3050
$\nu_s(CH)$	2925	2958	2962, 2948	2915
$\nu_{as}(NO_2)$	1558	1574	1561	1570
$\nu_s(NO_2)$	1383	1375	1374	1377
$\delta_a(CH_3)$	1436	1436	1438, 1426	1422
$\delta_s(CH_3)$	1423	1419	1409, 1405	1407
$r(CH_3)$	1092	1103	1104	1103

[a] Reference 40. [b] References 16 and 17.

Infrared Reflection Absorption Spectroscopy. Infrared data obtained following a saturation coverage of nitromethane on the thin-film oxide at 100 K is consistent with molecular adsorption, based on correspondence to the spectrum for the multilayer, to nitromethane on other surfaces,[16,17,19] and to condensed nitromethane[40] (Figure 2and Table 2). All vibrational assignments are made by comparison with the literature. The assignment of the spectrum obtained at 100 K in terms of intact nitromethane is also consistent with the observation of molecular desorption at 180 K. Aside from the peaks assigned to nitromethane, there is an additional feature at 1590 cm^{-1} that cannot be assigned to any normal modes of nitromethane. Although a definitive assignment of this peak is not possible, a similar peak was assigned to ν(N═O) of nitrosomethane (CH_3-NO) following nitromethane adsorption on Pt(111).[19]

Heating the CH_3NO_2-dosed surface to 300 K results in dissociation of the N−O bonds. All vibrational features associated with intact CH_3NO_2 disappear upon heating to 300 K, and there is no development of new peaks that would signify the

presence of intact N−O bonds (Figure 2). Specifically, there are no peaks between 1500 and 1900 cm^{-1}, the region for stretching modes in NO adsorbed on oxygen-modified Mo(110),[41] or in regions characteristic of NO_2—$\delta_s(NO_2)$ near 800 cm^{-1} and $\nu(NO_2)$ between 1180 and 1250 cm^{-1}—based on data for NO_2 on Au(111).[42]

The dissociation of N−O bonds at 300 K leads to the deposition of terminally bound oxygen (Mo═O) on the thin-film oxide, as signified by the peak at 981 cm^{-1} (Figure 2a). This peak is attributed to a Mo═O species, based on its close frequency match and similar dependence on temperature to previously characterized Mo═O species on the thin-film oxide.[37] This peak splits and redistributes intensity upon heating, to evolve into peaks at 984, 999, and 1020 cm^{-1} at 800 K (Figure 2a, inset). The intensity redistribution and shifts in peak positions are attributed to changes in the local environment of Mo═O moieties and in the morphology of the thin-film oxide, as previously demonstrated.[37] Notably, the persistence of these peaks to 800 K where product evolution is complete, and the invariance in their frequencies for $^{13}CH_3NO_2$, CH_3NO_2, and CD_3NO_2 confirm that neither C nor H contribute to these peaks (Figure 2a, inset). These results rule out any contribution from ν(CO) of methoxy (CH_3O), which has been observed in the same frequency range on oxygen-modified Mo(110).[38]

Nitromethane reaction on an ^{18}O-labeled thin-film oxide indicates that there is displacement of surface oxygen into terminal sites by ^{16}O deposited from CH_3NO_2. Peaks characteristic of both ν(Mo═^{18}O) at 950 and 975 cm^{-1}, and ν(Mo═^{16}O) at 997 and 1016 cm^{-1} are observed when CD_3NO_2 reacts on the ^{18}O-thin-film oxide (Figure 2a, inset). The degree of oxygen exchange depends on the temperature of the CD_3NO_2-dosed surface. At 300 K, only ν(Mo═^{16}O) at 981 cm^{-1} is observed, while both ν(Mo═^{18}O) at 939 cm^{-1} and ν(Mo═^{16}O) at 983 cm^{-1} are observed at 500 K, with the Mo═^{16}O species having the greater intensity (data not shown). As the surface temperature is increased to 800 K, peaks arising from Mo═^{18}O (950 and 975 cm^{-1}) have intensities almost twice that of Mo═^{16}O (997 and 1016 cm^{-1}). These results are consistent with the facile exchange of oxygen on Mo(110) reported in our earlier studies.[37]

In addition to Mo═O moeities, the species that ultimately yields HCN and H_2O is present between 300 and 500 K and is assigned as a methylimido intermediate (CH_3N). All modes observed in the infrared spectra, aside from ν(Mo═O), can be accounted for by a CH_3N species. The peak from ν(CN) of CH_3N is at 1290 cm^{-1}, which is close to the C−N stretch frequency of 1281 cm^{-1} reported for methylimide in $Os(NCH_3)(CH_2SiMe_3)_4$.[43] Furthermore, this peak shifts to 1275 cm^{-1} for $^{13}CH_3NO_2$ (Figure 3), in agreement with the 17 cm^{-1} downshift in ν(CN) observed upon ^{13}C isotopic substitution in gaseous CH_3N radicals,[44] and the 19 cm^{-1} downshift predicted using a harmonic oscillator approximation for a C−N stretch of CH_3N. The observation of $\bullet CH_3$ desorption commencing at 550 K is also consistent with the formation of CH_3N between 300 and 500 K. Methylimido has previously been identified on Pt(111) via decomposition of adsorbed trimethylamine, with ν(CN) reported at 1162 cm^{-1}.[45]

Other possible intermediates, namely methylene amidogen (CH_2N) and aminomethylidyne (CNH_2), are ruled out based on the absence of detectable dehydrogenation up to the onset of HCN production. The C═N stretch for a CH_2N species is generally in the range 1500−1750 cm^{-1}, as previously observed on Pt(111)[45] and Mo(110).[33] No peaks are detected in this region of the infrared spectra obtained after heating the CH_3NO_2-dosed surface to 300 K and above. While the C−N stretch in aminomethylidyne has been observed on Pt(111)[46,47] and Rh(111)[48] near 1300 cm^{-1}, the same as ν(CN) observed herein; there is no evidence in the infrared data for N−H bond formation between 300 and 500 K. The absence of peaks around 3300 cm^{-1}, the N−H stretching region, and in the range expected for $\delta(NH_2)$ (∼1500−1600 cm^{-1}), suggests that the intermediate contains no intact N−H bonds.

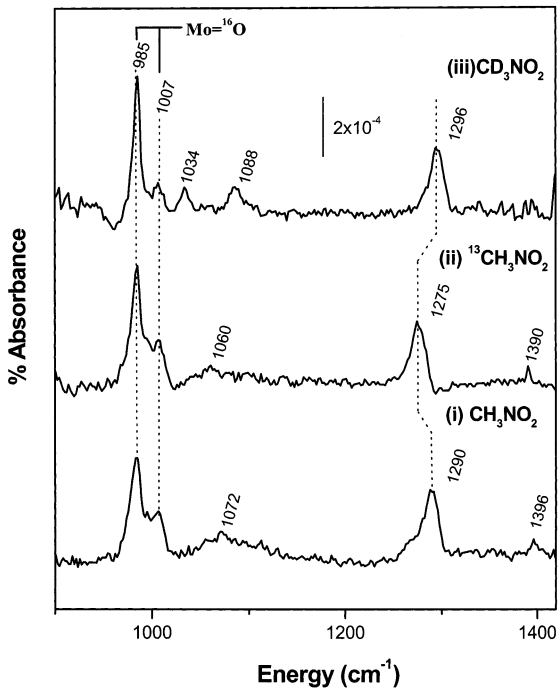

Figure 3. Infrared reflection absorption spectra obtained after heating isotopomers of nitromethane to 500 K: (i) CH_3NO_2, (ii) $^{13}CH_3NO_2$, and (iii) CD_3NO_2. A saturation coverage was initially adsorbed at 100 K and heated to 500 K using the same heating profile as for temperature-programmed reaction.

TABLE 3: Vibrational Bands (cm^{-1}) for CH_3NO_2, $^{13}CH_3NO_2$, and CD_3NO_2 Adsorbed on the Mo(110) Thin-Film Oxide at 100 K, and Heated to 500 K[a]

normal mode	CH_3NO_2	$^{13}CH_3NO_2$	CD_3NO_2	CH_3N on Pt(111)[b]
$r(CH_3)$	1072	1060	1034	
ν(CN)	1290	1275	1296	1162
$\delta_s(CH_3)$	1396	1390	1088	
$\delta_a(CH_3)$				1415
ν_s(CH)	2906	2900	2050	2956
$2\delta_s(CH_3)$	2845	2841	-	3061

[a] Comparison to the vibrational modes for CH_3N on Pt(111) is shown. [b] HREELS data from ref 45.

Other modes characteristic of a CH_3N intermediate are the methyl rocking mode at 1072 cm^{-1}, the deformation mode at 1396 cm^{-1}, and two distinct peaks in the C−H stretching region at 2906 and 2844 cm^{-1} (Figure 2). All of these modes shift as expected upon ^{13}C isotopic substitution and deuteration of nitromethane, with the exception that only one peak in the C−D stretching region at 2050 cm^{-1} is observed for CD_3N (Table 3). We assign the peaks at 2906 and 2900 cm^{-1} for CH_3N and $^{13}CH_3N$, respectively, as the symmetric C−H stretch. The lower intensity peaks at 2845 (CH_3N) and 2841 cm^{-1} ($^{13}CH_3N$) are assigned to overtones of the methyl deformation mode at ∼1400 cm^{-1}, most likely in combination with the symmetric C−H stretch. Previous studies of methoxy on Mo(110)[49] and Cu(111)[50] have identified strong Fermi resonances between overtones of $\delta(CH_3)$ and the C−H stretch. These resonances result in intensity borrowing by the overtone from the C−H

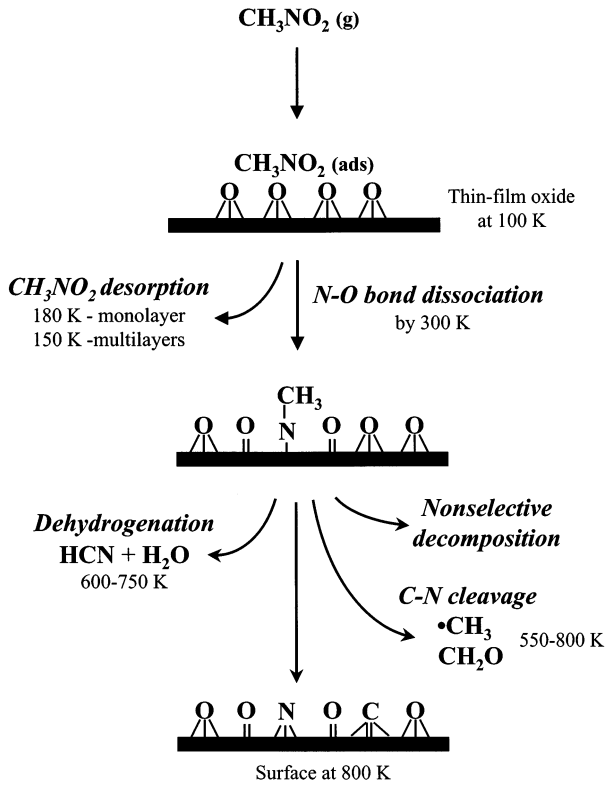

Figure 4. Proposed reaction scheme for nitromethane on the thin-film oxide formed on Mo(110).

stretch, such that significant intensity is observed in the overtone despite a weak oscillator strength in the deformation fundamental.[49] The fact that no overtone of $\delta(CD_3)$ is observed for CD_3N is consistent with our assignment, since the large energy separation between ν(CD) and $2\delta(CD_3)$, $\Delta E \sim 130$ cm^{-1}, would reduce the anharmonic coupling between these two modes. (The corresponding ΔE values for CH_3N and $^{13}CH_3N$ are ~ 50 cm^{-1}.)

There are anomalous shifts in the ν(CN) peaks, which indicate the presence of mode-coupling in the methylimido intermediate. The ν(CN) for CD_3N is higher in energy than that in either CH_3N and $^{13}CH_3N$: 1296 cm^{-1} for CD_3N compared to 1290 and 1275 cm^{-1} for CH_3N and $^{13}CH_3N$, respectively (Figure 3 and Table 3). This inverse isotopic effect is attributed to a difference in intramolecular coupling in CD_3N. We propose that the ν(CN) and $\delta(CH_3)$ modes, which are close in energy for the ^{12}C and ^{13}C intermediates, couple strongly. An out-of-phase transition of the dynamic dipole associated with these coupled modes would then lead to a *reduction* in their observed frequencies. In CD_3N, the coupling is reduced by the isotopic shift of $\delta(CD_3)$ to 1088 cm^{-1}; hence, the C−N stretch in CD_3N is restored to its higher, uncoupled frequency. There is precedence for mode-coupling in gas-phase methylimido radicals, which leads to anomalous shifts in the C−N stretch upon deuteration of the radicals.[44] In gaseous CH_3N, the C−N stretch and hydrogen umbrella modes occur at 1040 and 1349 cm^{-1}, respectively. In gaseous CD_3N, however, the deuterium umbrella mode shifts to 941 cm^{-1} and couples in-phase with the C−N stretch, thus pushing ν(CN) to 1110 cm^{-1}, which is ~ 70 cm^{-1} above that for gaseous CH_3N.

Discussion

Nitromethane reacts by dissociation of the N−O bonds below 300 K, to yield CH_3N_{ads}, and to deposit oxygen primarily in terminal sites on the thin-film oxide formed on Mo(110) (Figure 4). The vibrational data at 300 K is consistent with a CH_3N species that yields all products formed during temperature programmed reaction of CH_3NO_2. Subsequent dehydrogenation of CH_3N leads to HCN and water production at 695 K. Water is formed from reaction of surface oxygen with hydrogen produced during C−H bond scission. The production of water must be reaction-limited because water is formed from reaction of hydroxyls with hydrogen on the thin-film oxide at $\sim$225 K.[38] The correspondence in peak temperatures and line shapes for HCN and H_2O, and the isotopic shift to higher temperatures for DCN and D_2O production from CD_3NO_2, provide further evidence that both products are formed via the same rate-limiting step of C−H(D) bond scission.

Methyl radical evolution between 550 and 800 K indicates that homolytic C−N bond cleavage competes with dehydrogenation in CH_3N. Although gaseous $\bullet CH_3$ evolution from a surface reaction is precedented in methoxy decomposition on oxidized Mo(110),[38] methoxy cannot account for $\bullet CH_3$ evolution from nitromethane. No methoxy, which would be characterized by a strong ν(CO) between 960 and 980 cm^{-1},[38,51] is identified on the bases of infrared data. Moreover, $\bullet CH_3$ production from nitromethane peaks at $\sim$50 K higher than that from methoxy on the thin-film oxide and is consistent with the higher thermal activation needed to break the stronger C−N bond, compared to C−O in methoxy.[49,52,53] Once formed, some methyl radicals are proposed to add to surface oxygen to yield transient methoxy, which would rapidly eliminate to formaldehyde. Methoxy is known to form by direct addition of $\bullet CH_3$ to oxygen in quasi-3-fold sites on Mo(110);[51] thus, the prevalence of $CH_2{}^{18}O$ over $CH_2{}^{16}O$ production on ^{18}O-labeled thin-film oxide, where the majority of high-coordination sites are occupied by ^{18}O, is consistent with a methoxy precursor to formaldehyde.

The products of nitromethane reaction on the thin-film oxide are qualitatively similar to those on Pt(111),[19] and clean and oxygen-covered Ni(111),[20] in that N−O bond dissociation predominates and the majority of C−N bonds are retained. On all these surfaces, the major product is HCN, which is formed together with a dehydrogenation product, namely, H_2O or H_2. As on oxidized Mo(110), no NO reduction products are observed from the Pt and Ni surfaces. In contrast, nitromethane shows no thermally activated reaction on Au(111)[17] and Sn/Pt(111) surface alloys.[18] The lack of reaction on Au is consistent with the low activation energy for molecular CH_3NO_2 binding to this surface, and the absence of a strong thermodynamic driving force for Au−O bond formation. In the case of Sn/Pt(111) alloys, addition of Sn suppresses the reactivity of Pt(111) toward N−O bond dissociation in nitromethane, despite the fact that bulk Sn is more oxophilic than Pt. This is attributed to an increased kinetic barrier to dissociation on the alloys, caused by changes in the surface electronic structure arising from bonding interactions between Pt and Sn.[18]

The interaction of nitromethane with oxophilic metals clearly alters the reaction pathways from homogeneous nitromethane reactions. Isomerization to methyl nitrite—the dominant pathway for gas-phase nitromethane—has not been observed on all transition metal surfaces studied to date, including the weakly interacting Au(111) surface.[17] Isomerization on the thin-film oxide on Mo(110) is also ruled out based on comparison to methyl nitrite reaction on oxidized Mo(110).[54] Methyl nitrite decomposes to NO and adsorbed methoxy upon adsorption at 110 K on oxidized Mo(110); hence, the fact that no NO and methoxy are detected in CH_3NO_2 reaction on the thin-film oxide confirms that rearrangement to CH_3ONO does not occur.

The reaction of nitromethane on the thin-film oxide on Mo(110) does not lead to significant amounts of products desired

in the CH_4-assisted reduction of NO, namely C-oxygenates, and N_2 or N_2O. The production of some $\bullet CH_3$ and CH_2O indicates that C−N bond activation is a minor pathway in nitromethane reaction on the thin-film oxide. Unfortunately, the accompanying NO reduction yields N_2 at high temperature via atom recombination. This is attributed to the strong driving force for N-chemisorption to the Mo(110) surface following C−N bond scisison, as reflected in the high temperature (∼1250 K) required for N-recombination to N_2.

The propensity for nitromethane to decompose by loss of oxygen to the surface is due to the strong driving force for Mo−O bond formation, in conjunction with the presence of a significant number of oxygen vacancies, and the low oxidation state of our thin-film oxide. Notably, NO itself readily loses oxygen, yielding reduction products (N_2 and N_2O) at temperatures below 300 K on this surface.[41] It is possible that N−O bond retention in nitromethane may be favored on a more highly oxidized surface with fewer vacancies; this will be the subject of a later study.

Taken together, there is no evidence in the studies of nitromethane reactions to date that CH_3NO_2 leads to a substantial amount of NO reduction. This, however, does not preclude the possibility that an intermediate similarly containing carbon, nitrogen and oxygen may be formed in the CH_4 + NO reaction. Ideally, the selectivity of this intermediate toward producing CH_2O and/or other carbon-containing oxgenates would be higher than in nitromethane. Under catalytic conditions, oxygen vacancies created when oxygenates desorb from the catalyst surface would provide active metal sites for NO reduction via N−N coupling. On this basis, studies on the interactions of other C,N,O-containing molecules, e.g., nitrosomethane and formamide, with model catalyst substrates may help elucidate the elementary steps important to the CH_4-assisted reduction of NO.

Conclusions

Nitromethane decomposes via dissociation of the N−O bonds on the thin-film oxide formed on Mo(110), which is similar to the chemistry on Pt(111) and Ni surfaces. After N−O bond scission by 300 K, surface-bound CH_3N and Mo═O moeities are formed. The majority of CH_3N dehydrogenates at ∼600 K to yield HCN and H_2O, although some C−N bond scission also occurs to evolve $\bullet CH_3$. Direct addition of methyl radicals to surface oxygen forms transient methoxy, which rapidly eliminates to formaldehyde. The prevalence of C−N bond retention suggests that nitromethane is not a likely intermediate in the CH_4-assisted reduction of NO. The high coverage of oxygen on Mo(110) affects the chemistry of nitromethane in two distinct ways: (1) oxygen scavenges hydrogen that is produced in dehydrogenation pathways, subsequently removing it as water, and (2) oxygen adds directly to gaseous methyl radicals to form formaldehyde.

Acknowledgment. The authors acknowledge the U.S. Department of Energy, Basic Energy Sciences, for support of this work under Grant DE-FG02-84-ER13289. A.S.Y.C. thanks the Harvard Materials Research Science and Engineering Center (MRSEC) for the award of a Fellowship, and Ilona Kretzschmar for helpful discussions.

References and Notes

(1) Parvulescu, V. I.; Grange, P.; Delmon, B. *Catal. Today* **1998**, *46*, 233−316.
(2) Hasenberg, D.; Schmidt, L. D. *J. Catal.* **1987**, *104*, 441−453.
(3) Bodke, A. S.; Olschki, D. A.; Schmidt, L. D. *Appl. Catal. A* **2000**, *201*, 13−22.
(4) Cant, N. W.; Cowan, A. D.; Liu, I. O. Y.; Satsuma, A. *Catal. Today* **1999**, *54*, 473−482.
(5) Cant, N. W.; Liu, I. O. Y. *Catal. Today* **2000**, *2131*, 1−14.
(6) Lombardo, E. A.; Sill, G. A.; d'Itri, J. L.; Hall, W. K. *J. Catal.* **1998**, *173*, 440−449.
(7) Lukyanov, D. B.; Lombardo, E. A.; Sill, G. A.; d'Itri, J. L.; Hall, W. K. *J. Catal.* **1996**, *163*, 447−456.
(8) Gaudin, C.; Duprez, D.; Mabilon, G.; Prigent, M. *J. Catal.* **1996**, *160*, 10−18.
(9) Li, Y.; Slager, T. L.; Armor, J. N. *J. Catal.* **1994**, *150*, 388−399.
(10) Cant, N. W.; Cowan, A. D. *Catal. Today* **1997**, *35*, 89−95.
(11) Zhang, X.; Walters, A. B.; Vannice, M. A. *J. Catal.* **1994**, *146*, 568−578.
(12) Fokema, M. D.; Ying, J. Y. *Catal. Rev.* **2001**, *43*, 1−29.
(13) Ansell, G. P.; Golunski, S. E.; Hayes, J. W.; Walker, A. P.; Burch, R.; Millington, P. J. *Stud. Surf. Sci. Catal.* **1995**, *96*, 577−590.
(14) Cowan, A. D.; Cant, N. W.; Haynes, B. S.; Nelson, P. F. *J. Catal.* **1998**, *176*, 329−343.
(15) Cant, N. W.; Cowan, A. D.; Doughty, A.; Haynes, B. S.; Nelson, P. F. *Catal. Lett.* **1997**, *46*, 207−212.
(16) Nandi, S.; Arnold, P. A.; Carpenter, B. K.; Nimlos, M. R.; Dayton, D. C.; Ellison, G. B. *J. Phys. Chem. A* **2001**, *105*, 7514−7524.
(17) Wang, J.; Bansenauer, B. A.; Koel, B. E. *Langmuir* **1998**, *14*, 3255−3263.
(18) Peck, J. W.; Mahon, D. I.; Beck, D. E.; Koel, B. E. *Surf. Sci.* **1998**, *410*, 170−188.
(19) Saliba, N.; Wang, J.; Bansenauer, B. A.; Koel, B. E. *Surf. Sci.* **1997**, *389*, 147−161.
(20) Benziger, J. B. *Appl, Surf. Sci.* **1984**, *17*, 309−323.
(21) Benziger, J. B. *Combust. Sci. Technol.* **1982**, *29*, 191−205.
(22) Hwang, S. Y.; Kong, A. C. F.; Schmidt, L. D. *Surf. Sci.* **1989**, *217*, 179−198.
(23) Levoguer, C. L.; Nix, R. M. *J. Chem. Soc., Faraday Trans.* **1997**, *93*, 1813−1820.
(24) Crawforth, C. G.; Waddington, D. J. *Trans. Faraday Soc.* **1969**, *65*, 1334.
(25) Perche, A.; Tricot, J. C.; Lucquin, M. *J. Chem. Res. (S)* **1979**, 116−117.
(26) Wang, J.; Brower, K. R. *J. Org. Chem.* **1997**, *62*, 9048−9054.
(27) Dewar, M. J. S.; Ritchie, J. P.; Alster, J. *J. Org. Chem.* **1985**, *50*, 1031−1036.
(28) Wodtke, A. M.; Hintsa, E. J.; Lee, Y. T. *J. Chem. Phys.* **1986**, *84*, 1044−1045.
(29) Burch, R.; Watling, T. C. *Appl. Catal. B* **1997**, *11*, 207−216.
(30) Yao, H. C.; Rothschild, W. G.; Gandhi, H. S. *Stud. Surf. Sci. Catal.* **1984**, *19*, 71−75.
(31) Halasz, I.; Brenner, A.; Shelef, M. *Catal. Lett.* **1993**, *22*, 147−156.
(32) Wiegand, B. C.; Uvdal, P. E.; Serafin, J. G.; Friend, C. M. *J. Am. Chem. Soc.* **1991**, *113*, 6686−6687.
(33) Weldon, M. K.; Friend, C. M. *Surf. Sci.* **1994**, *310*, 95−102.
(34) Liu, A. C.; Friend, C. M. *Rev. Sci. Instrum.* **1986**, *57*, 1519−1522.
(35) Colaianni, M. L.; Chen, J. G.; Weinberg, W. H.; Yates, J. T. *Surf. Sci.* **1992**, *279*, 211−222.
(36) Queeney, K. T.; Friend, C. M. *J. Phys. Chem. B* **1998**, *102*, 5178−5181.
(37) Nart, F. C.; Kelling, S.; Friend, C. M. *J. Phys. Chem. B* **2000**, *104*, 3212−3218.
(38) Queeney, K. T.; Friend, C. M. *J. Chem. Phys.* **1998**, *109*, 6067−6074.
(39) Weldon, M. K.; Friend, C. M. *Rev. Sci. Instrum.* **1995**, *66*, 5192−5195.
(40) Matyshak, V. A.; Ukharskii, A. A.; Il'ichev, A. N.; Sadykov, V. A.; Korchak, V. N. *Kinet. Catal.* **1999**, *40*, 105−111.
(41) Queeney, K. T.; Friend, C. M. *J. Phys. Chem. B* **1998**, *102*, 9251−9257.
(42) Wang, J.; Koel, B. E. *J. Phys. Chem. B* **1998**, *102*, 8573−8579.
(43) Marshman, R. W.; Shapley, P. A. *J. Am. Chem. Soc.* **1990**, *112*, 8369−8378.
(44) Chappell, E. L.; Engelking, P. C. *J. Chem. Phys.* **1988**, *89*, 6007−6016.
(45) Erley, W.; Xu, R.; Hemminger, J. C. *Surf. Sci.* **1997**, *389*, 272−286.
(46) Jentz, D.; Celio, H.; Mills, P.; Trenary, M. *Surf. Sci.* **1995**, *341*, 1−8.
(47) Jentz, D.; Mills, P.; Celio, H.; Trenary, M. *Surf Sci* **1996**, *368*, 354−360.
(48) Bol, C. W. J.; Kovacs, J. D.; Chen, M.; Friend, C. M. *J. Phys. Chem. B* **1997**, *101*, 6436−6442.
(49) Uvdal, P.; Weldon, M. K.; Friend, C. M. *Phys. Rev. B* **1994**, *50*, 12258−12261.
(50) Chesters, M. A.; McCash, E. M. *Spectrochimica Acta A* **1987**, *43*, 1625−1630.

(51) Queeney, K. T.; Chen, D. A.; Friend, C. M. *J. Am. Chem. Soc.* **1997**, *119*, 6945−6946.
(52) Hadjebar, I.; Nait Achour, M.; Boucekkine, A.; Berthier, G. *Chem. Phys.* **2001**, *264*, 153−161.
(53) Gonzalez, G.; Schlegel, H. B. *J. Am. Chem. Soc.* **1992**, *114*, 9118−9122.
(54) Deiner, L. J.; Wilke, S. L.; Friend, C. M.; Nart, F. C. *Surf. Sci.* **2001**, *477*, L301-L307.